SIAM J. SCI. COMPUT.
Vol. 26, No. 4, pp. 1166–1191


# LOCALLY DIVERGENCE-PRESERVING UPWIND FINITE VOLUME SCHEMES FOR MAGNETOHYDRODYNAMIC EQUATIONS*

MANUEL TORRILHON†

**Abstract.** A main issue in nonstationary, compressible magnetohydrodynamic (MHD) simulations is controlling the divergence of the magnetic flux. This paper presents a general procedure showing how to modify the intercell fluxes in a conservative MHD finite volume code such that the scheme becomes locally divergence preserving. That is, a certain discrete divergence operator vanishes exactly during the entire simulation, which results in the suppression of any divergence error. The procedure applies to arbitrary finite volume schemes provided they are based on intercell fluxes. We deduce the necessary modifications for numerical methods based on rectangles and triangles and present numerical experiments with the new schemes.

The theoretical justification of the schemes is given in two independent ways. One way starts with the discrete divergence operator that has to be preserved and modifies the fluxes accordingly. The second way uses a finite element reconstruction via Nedelec elements. Both methods lead to equivalent numerical methods.

**Key words.** magnetohydrodynamics, finite volume methods, divergence constraint, Nedelec elements

**AMS subject classifications.** 76W05, 65M06

**DOI.** 10.1137/S1064827503426401

## 1. Introduction.

The magnetic flux density $\mathbf{B}$ in magnetohydrodynamic (MHD) simulations is subject to the constraint $\operatorname{div}\mathbf{B} = 0$. This expresses the fact that there are no magnetic monopoles. In the analytical solutions of the equations this divergence constraint has to be imposed only on the initial conditions. Afterwards, the evolution equation takes care that the divergence will be preserved for later times. This divergence preservation is an inherent analytical property of the evolution operator of the magnetic field. In numerical discretizations the preservation property is not attained in general. Thus, one major task in the design of numerical methods for magnetohydrodynamics is the control of the divergence errors. Especially in compressible MHD calculations, divergence errors are generated and amplified by possible discontinuities; see, e.g., [5]. These errors usually accumulate and lead to a breakdown of classical numerical schemes, making it impossible to calculated MHD solutions with those methods.

Most applications of magnetohydrodynamics is found in astrophysics, e.g., in solar physics [9] or space weather prediction [12]. MHD flows are also of interest in the investigation of electric propulsion devices, e.g., in [23]. Industrial applications are given in the simulation of electric arcs, e.g., in current breakers [17].

The construction of divergence-free methods for magnetohydrodynamics is discussed extensively in the literature. We may distinguish between three major approaches. The first one, originally described by Brackbill and Barnes in [5], uses a classical numerical method but cleans the field of the magnetic flux density after every time step or after a certain number of time steps. The cleaning is obtained by solving an elliptic equation for a scalar field whose gradient will correct $\mathbf{B}$ such

*Received by the editors April 23, 2003; accepted for publication (in revised form) March 18, 2004; published electronically March 11, 2005.
http://www.siam.org/journals/sisc/26-4/42640.html
†ETH Zurich, Seminar for Applied Mathematics, CH-8092 Zürich, Switzerland (manuel@math.ethz.ch).

that $\operatorname{div} \mathbf{B} = 0$. This method leads to solenoidal fields during the calculation and avoids divergence errors. However, the method is expensive due to the solution of a global elliptic equation. Moreover, inspection of the analytical equation shows that the preservation of the divergence *is not connected to an elliptic problem.* Analytically, the divergence is locally preserved, and it should be possible to construct a locally divergence-preserving numerical method as well.

The second approach constructs divergence-free methods by special discretization of the evolution equation of $\mathbf{B}$. Originally described by Evans and Hawley in [13], these ideas were used and further developed by Balsara and Spicer [4], as well as by Dai and Woodward [8]. Again, in those methods a correction step follows each time step of a classical numerical method. This correction step provides a divergence-preserving evolution for the magnetic flux density on a staggered grid. The correction character and the staggered grid appear as disadvantages since they leave the cell average approach in the finite volume method. In [34] Toth showed that the staggered grid may be eliminated by explicit extrapolation and interpolation. The apparent restriction of the staggered approach to structured meshes is relaxed by De Sterck in [11] and in a very recent paper [3] by Balsara.

The third approach is due to Powell [30], who constructed a modified analytical MHD system based on the assumption that $\operatorname{div} \mathbf{B} \neq 0$. This new system contains additional terms which advect the divergence errors out of the computational domain. Dedner et al. [10] and Munz et al. [27] improve and generalize Powell's ideas for MHD as well as for electrodynamics on unstructured grids.

This paper will construct conservative finite volume methods for compressible magnetohydrodynamics that are locally divergence-preserving on rectangular and triangular grids. We consider only the ideal equations since they usually represent the building block also for dissipative MHD simulations. We concentrate on the cell average approach of conservative finite volume schemes. The conservation in the sense of volume integrals is a crucial property of numerical methods for conservation laws since it assures the approximation of the right weak solutions. For the incorporation of the local divergence preservation we use the flux distribution framework given in [33]. Flux distributions are piecewise constant basis shape functions in the grid for which a given discrete constraint vanishes. The update in a numerical scheme has to be built out of linear combinations of such flux distributions in order to provide constraint preservation. We demonstrate the flux distributions for divergence preservation and give the necessary modifications for finite volume fluxes. Hence, the divergence preservation will be incorporated directly into the fluxes of the scheme, reproducing the analytical preservation properties of the evolution. As a result the values of the discrete divergence operator given later in (12) will stay exactly the same during the entire calculation. Since the scheme is based only on special distributions of intercell fluxes, any finite volume scheme can be modified into a locally divergence-preserving scheme. Several numerical examples demonstrate the capabilities of the modified schemes on rectangular and triangular grids. A special case of the scheme obtained on rectangular grids can be related to a staggered grid method used in [4] and [34].

Additionally, we will present an alternative construction of the presented scheme, which was inspired by the work of De Sterck in [11]. It uses a special projection of a finite element reconstruction of the residual in the numerical method. The key issue is the use of the Stokes formulation of the evolution equation for $\mathbf{B}$ and Nedelec or face elements for reconstruction. Surprisingly, this deduction leads to the same

divergence-preserving schemes as the modification of the flux distributions. However, the construction via so-called Nedelec averaging does not provide the knowledge of an exactly preserved discrete divergence operator on the cell averaged values.

Though the numerical schemes in this paper are constructed for magnetohydrodynamics, the result may be interesting for other fields of computational physics where evolution equations with constraints are present. In the vorticity method for calculating incompressible flows, e.g., in [18], or in climatological flows, e.g., in [25], staggered schemes are used for constraint preservation. In general relativity the Einstein equations are subject to constraints which are important to control in numerical simulations; see, e.g., [7] and [1]. However, the constraints of Einstein's equations are nonlinear, a case which is not covered by this paper. Numerical methods for vorticity-preserving equations are also discussed in [26].

The remainder of the paper is organized as follows: After we briefly introduce the equations of magnetohydrodynamics in section 2, the general ideas of flux distributions are summarized in section 3. In the next two sections, possible flux distributions for rectangular (section 4) and triangular (section 5) grids are presented. Furthermore, in these sections we construct the modifications of finite volume schemes for the respective grids and provide numerical experiments. Section 6 is devoted to the alternative construction of the presented schemes by finite element tools.

**2. MHD equations.** The equations of ideal magnetohydrodynamics consider the conservative variables density $\rho$, momentum density $\rho\mathbf{v}$, energy density $E$, and magnetic flux density (also magnetic field, for short) $\mathbf{B}$ to describe the flow of a plasma. As a system of field equations, we have

$$
\begin{aligned}
\partial_t \rho &+ \operatorname{div} \rho\mathbf{v} &&= 0,\\
\partial_t \rho\mathbf{v} &+ \operatorname{div} \left( \rho \mathbf{v}\,\mathbf{v}^T + \left( p + \frac{1}{2}\mathbf{B}^2 \right) \mathbf{I} - \mathbf{B}\,\mathbf{B}^T \right) &&= 0,\\
\partial_t E &+ \operatorname{div} \left( \left( E + p + \frac{1}{2}\mathbf{B}^2 \right) \mathbf{v} - \mathbf{B}\,\mathbf{B}^T\,\mathbf{v} \right) &&= 0,\\
\partial_t \mathbf{B} &+ \operatorname{div} \left( \mathbf{B}\,\mathbf{v}^T - \mathbf{v}\,\mathbf{B}^T \right) &&= 0,
\end{aligned}
\tag{1}
$$

that is, the balance laws of mass, momentum, and energy and the induction equation. The system is closed by the equation of state of an ideal plasma $E = \frac{1}{\gamma-1} p + \frac{1}{2}\rho\mathbf{v}^2 + \frac{1}{2}\mathbf{B}^2$, where $\gamma$ is the adiabatic coefficient of the plasma. The system (1) forms a hyperbolic system of conservation laws (see, e.g., [20] for hyperbolic properties), a fact which suggests using a conservative finite volume scheme in nonstationary MHD flow simulations.

The difficulty of such simulations lies in handling the intrinsic constraint which follows from rewriting the induction equation $(1)_4$ with a curl, so that we have

$$
\partial_t \mathbf{B} + \operatorname{curl} (\mathbf{B} \times \mathbf{v}) = 0 \qquad \Rightarrow \qquad \operatorname{div} \mathbf{B} = \text{const in time}. \tag{2}
$$

This means that the divergence of the magnetic flux density remains untouched during the evolution. Since the magnetic flux density has to be solenoidal in the initial conditions, it follows that it will be divergence-free for all times. However, the solenoidal magnetic flux density should not be seen as the main issue. It is the *update* or *residual* in the numerical method that has to be divergence-free. Thus, the main problem is to construct numerical methods that preserve the divergence during the evolution irrespective of the actual divergence of the field that is evolved. The solenoidal magnetic flux density, then, is a problem only for the initial data.

This paper deals mainly with the numerical representation of the induction equation (2). Nevertheless, we should think of this equation as being embedded in a finite volume scheme, and we should keep in mind that, e.g., intercell fluxes are defined and calculated only for the complete system (1).

We restrict ourselves to the two-dimensional case. The extension of the presented algorithms to three dimensions is possible; see section 6. In two dimensions the divergence of the magnetic flux density is influenced only by the components $B^{(x)}$ and $B^{(y)}$. Hence, the evolution of $B^{(z)}$ is not of interest for the divergence preservation. Still, the component $B^{(z)}$ need not be zero in a two-dimensional calculation. This is sometimes referred to as 2.5 dimensions. The important part of the induction equation reduces to the system

$$\begin{aligned} \partial_t B^{(x)} + \partial_y (B^{(x)} v^{(y)} - B^{(y)} v^{(x)}) &= 0, \\ \partial_t B^{(y)} - \partial_x (B^{(x)} v^{(y)} - B^{(y)} v^{(x)}) &= 0, \end{aligned} \tag{3}$$

whose fluxes are governed by the single function

$$f(\mathbf{B}, \mathbf{v}) = B^{(x)} v^{(y)} - B^{(y)} v^{(x)}. \tag{4}$$

Here we have used $\mathbf{v} = (v^{(x)}, v^{(y)}, v^{(z)})$ for the components of the velocity. Comparison with Maxwell's equations shows that $f(\mathbf{B}, \mathbf{v})$ represents the $z$-component of the electric field present in the plasma.

**3. General framework.** In [33] conservative finite volume methods for constrained advection in the form (2) have been developed that preserve discrete divergence operators exactly. Unfortunately, these methods cannot be used directly to obtain divergence preservation in the context of standard finite volume schemes. In [24] a variant the method of [33] was used in an MHD simulation based on the method of transport; see [14], [15], and [29].

However, the basic ideas developed in [33] also guide the way to constructing a locally divergence-preserving method based on a *standard finite volume method*. The focus on a finite volume description is important in obtaining a *conservative* method (in the sense of volume integrals) which additionally is locally divergence preserving. Conservation in the sense of volume integrals is the main condition for a method in order to converge to the true weak solution of a conservation law, as stated by the Lax–Wendroff theorem; see [16]. In the following, we summarize the general framework given in [33] in order to provide the necessary concepts.

We consider a domain $\Omega \subset \mathbb{R}^D$ and a time-dependent vector field $\mathbf{u} : \mathbb{R}^+ \times \Omega \to \mathbb{R}^D$ ($D$: space-dimension) obeying a generic evolution

$$\partial_t \mathbf{u} + \mathcal{F}(\mathbf{u}) = 0 \tag{5}$$

with transport operator $\mathcal{F}$. The generic constraint $\mathcal{C}$ is assumed to be intrinsic for (5); that is, the relation

$$\mathcal{C}(\mathcal{F}(\mathbf{u})) \equiv 0 \tag{6}$$

holds, which directly implies $\mathcal{C}(\mathbf{u}) = \text{const}$ in time for any solution of (5). We assume that the constraint is linear, which is fortunately the case in most applications, e.g., in magnetohydrodynamics. The case of nonlinear constraints needs special investigation. The computational domain $\Omega$ is covered by a grid $\mathcal{T} = \{K_i\}_{i=1,2,\ldots}$ with polygonal, nonoverlapping cells $K_i$ whose diameter is bounded by $h$. The set $\mathcal{N}(K)$ gives all neighboring cells of the cell $K$ joining a common face, edge, or vertex. A time discretization by $\Delta t$ leads to a cellwise constant grid function $\tilde{\mathbf{u}}^m : \mathcal{T} \to \mathbb{R}^D$ which approximates $\mathbf{u}$ after $m$ time steps by cell mean values.

**3.1. Constraint-preserving schemes.** The central quantity of constraint-preserving schemes is the so-called "flux distribution." It is the structure of the flux distribution that determines whether a certain scheme is constraint preserving or not.

DEFINITION 3.1 (flux distribution). *Given the space of vector-valued grid functions denoted by* $V = \left\{g : \mathcal{T} \to \mathbb{R}^D\right\}$*, we define a "flux distribution"* $\Phi_K : V \to V$ *which is attached to a grid cell* $K$ *and maps the grid function* $\tilde{\mathbf{u}}$ *into another grid function*

$$\Phi_K\left(\tilde{\mathbf{u}}\right) : \mathcal{T} \to \mathbb{R}^D, \tag{7}$$

*with* $\operatorname{supp}\Phi_K\left(\tilde{\mathbf{u}}\right) \subseteq \{K\} \cup \mathcal{N}\left(K\right)$*. The evaluation* $\Phi_K\left(\tilde{\mathbf{u}}\right)\big|_{\hat{K}}$ *gives the change of* $\tilde{\mathbf{u}}$ *at cell* $\hat{K}$ *caused by cell* $K$*, namely, the flux.*

A flux distribution is assigned to each cell of the grid and depends on the solution $\tilde{\mathbf{u}}$ in a local manner. The definition is more general than that of usual intercell fluxes, since it admits fluxes to any neighboring cell, especially across corners. This incorporates multidimensionality from the very beginning. Global conservation of $\tilde{\mathbf{u}}$ may be expressed by the statement that the integral of $\Phi_K\left(\tilde{\mathbf{u}}\right)$ over its support vanishes.

A certain form of the flux distribution and its dependency on $\tilde{\mathbf{u}}$ is usually constructed from consistency with the transport equation under consideration. Once the flux distribution is defined, an explicit evolution scheme follows by simply collecting contributions of all flux distributions of all cells, that is,

$$\tilde{\mathbf{u}}^{m+1}\big|_K = \tilde{\mathbf{u}}^m|_K + \sum_{\hat{K} \in \{K\} \cup \mathcal{N}(K)} \Phi_{\hat{K}}\left(\tilde{\mathbf{u}}^m\right)\big|_K . \tag{8}$$

Here the value of $\tilde{\mathbf{u}}$ in a cell $K$ is updated by contributions of all neighboring cells. The contributions are given by evaluations of flux distributions. The resulting scheme may be considered as a conservative finite volume scheme. Note that virtually any traditional finite volume scheme can be written in the form (8), and the flux distribution may then be identified; see also [33].

Since the constraint is assumed to be linear, we expect a discretization which may be written as matrix operation $\mathcal{C}\left(\mathbf{u}\right)\big|_K = \tilde{\mathcal{C}}_K \cdot \tilde{\mathbf{u}} + O\left(h^n\right)$ on the grid function $\tilde{\mathbf{u}}$, which follows from projection of $\mathbf{u}$. If preservation of the constraint should be achieved for scheme (8), then, as was shown in [33], we have to look for shape functions $\hat{\Phi}$ for flux distributions satisfying

$$\tilde{\mathcal{C}}_K \cdot \hat{\Phi}_{\hat{K}} = 0 \quad \forall K, \hat{K} \tag{9}$$

as a purely geometric condition. To some extent this is a discrete analogy to (6), which states that the constraint is intrinsic. See also [19], where discrete analogues of vector-analytic relations are considered.

As system (9) is homogeneous, we generally hope for a solution space from which we consider only an appropriate basis set of shape functions $\{\hat{\Phi}_K^{(g)}\}$ with $g = 1, 2, \ldots,$ all of which are constraint preserving. These shape functions form an appropriate basis for the solution space of (9). The final flux distribution has to be assembled from these solutions via

$$\Phi_K\left(\tilde{\mathbf{u}}\right) = \sum\nolimits_g \varphi_K^{(g)}\left(\tilde{\mathbf{u}}\right) \hat{\Phi}_K^{(g)} \tag{10}$$

with unknown coefficients $\varphi_K^{(g)}$, which give the amplitudes of the flux distributions. The representation (10) gives rise to the interpretation of $\hat{\Phi}_K^{(g)}$ as a shape function. Note that the choice of $\varphi_K^{(g)}$ does not affect the preservation of the constraint; see [33]. The expression for $\Phi_K$ enters scheme (8), and the remaining coefficients $\varphi_K^{(g)}$ have to follow from consistency.

**4. Rectangular grids.** We proceed now with constructing divergence-preserving schemes for magnetohydrodynamics on rectangular grids. Hence, the constraint is $\mathcal{C}(\cdot) = \operatorname{div}(\cdot)$. The cells are denoted by $K = (i, j)$ with positions $(x_i, y_j)$ and size $\Delta x \times \Delta y$. The geometry factor of the grid $\alpha = \frac{\Delta x}{\Delta y}$ shall be bounded from above and stay away from zero. In cases of accuracy considerations, we refer to $h = \max(\Delta x, \Delta y)$. Cell averages of $\mathbf{B}$ at time level $n$ are denoted by $\mathbf{B}_{i,j}^n$, omitting the tilde.

In what follows we will consider only flux distributions for the inner cells of the computational domain. In the numerical experiments boundaries are incorporated by extending the computational domain with ghost cells. This strategy turns out to be reliable. In principle, the boundary cells need a special treatment in which we consider one-sided divergence operators and construct divergence-preserving one-sided flux distributions. However, this remains for future work.

**4.1. Discrete divergence operators.** The possible flux distributions resulting from (9) depend on the form of the discrete operator $\tilde{\mathcal{C}}$. Hence, the crucial task in designing constraint-preserving numerical methods is the choice of the operator $\tilde{\mathcal{C}}$.

In [33] it was shown that the classical divergence operator on a rectangular grid

$$\operatorname{div}^{(0)} \mathbf{B}\Big|_{i,j} = \frac{B_{i+1,j}^{(x)} - B_{i-1,j}^{(x)}}{2\Delta x} + \frac{B_{i,j+1}^{(y)} - B_{i,j-1}^{(y)}}{2\Delta y} \tag{11}$$

admits only a single flux distribution, which does not give rise to practical schemes. However, there exists a three-parametric family of second-order divergence operators with a 3×3 stencil. The so-called extended operator $\operatorname{div}^{(\star)}$ given by

$$\operatorname{div}^{(\star)} \mathbf{B}\Big|_{i,j} = \frac{\{B_{i+1,j}^{(x)}\}_y - \{B_{i-1,j}^{(x)}\}_y}{2\Delta x} + \frac{\{B_{i,j+1}^{(y)}\}_x - \{B_{i,j-1}^{(y)}\}_x}{2\Delta y} \tag{12}$$

is singled out in this family as having the most compact flux distributions and a minimal error constant; see [33]. Here, curled brackets stand for

$$\begin{aligned} \{\psi_{i,j}\}_y &= \frac{1}{4}\left(\psi_{i,j+1} + 2\psi_{i,j} + \psi_{i,j-1}\right), \\ \{\psi_{i,j}\}_x &= \frac{1}{4}\left(\psi_{i+1,j} + 2\psi_{i,j} + \psi_{i-1,j}\right), \end{aligned} \tag{13}$$

i.e., averaging between vertical or horizontal cells. Like the classical operator, $\operatorname{div}^{(\star)} \mathbf{B}$ gives a second-order approximation to the divergence on cell $(i, j)$ using a 3×3 stencil. The difference lies only in the second-order residual terms. Taylor expansion around the cell $(i, j)$ leads to

$$\operatorname{div}^{(0)} \mathbf{B} + \frac{1}{8}\partial_{xy}^2(\Delta y^2 \partial_y B^{(x)} + \Delta x^2 \partial_x B^{(y)}) = \operatorname{div}^{(\star)} \mathbf{B} + \mathcal{O}\left(h^3\right). \tag{14}$$

It follows that the operators are equivalent up to second order for smooth solutions. Note that for nonsmooth solutions the operators (12) and (11) still yield a result

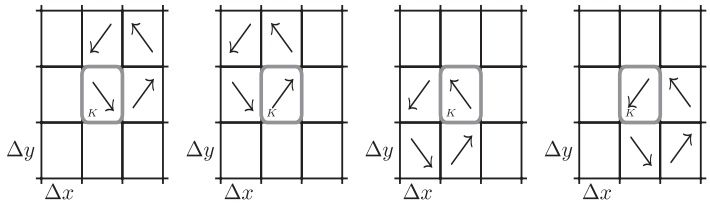


FIG. 1. *Sketches of the four possible flux distributions* $\Phi_K^{(1,2,3,4)}$ *of a cell* $K$ *that preserve the extended discrete divergence operator* $\operatorname{div}^{(\star)}$ *on a rectangular grid. Any change of the magnetic field in the grid must be represented by linear combinations of these flux distributions. Note that the flux distributions approximate closed curves, a fact that mirrors the physical interpretation of a vanishing divergence.*

consistent with the divergence in the distributional sense. Viewed as distribution, the divergence of a vector field maps a test function $\varphi \in \mathcal{D}$ to the real number $\varphi \mapsto \int_\Omega \mathbf{B} \operatorname{grad} \varphi$. Given a test function and an evaluation of the divergence operators $\operatorname{div}^{(\star,0)}$ on a possibly discontinuous vector field $\mathbf{B}$, we have consistency in the form

$$\lim_{h\to 0} \int_\Omega \varphi \operatorname{div}^{(\star,0)} \mathbf{B} = \int_\Omega \mathbf{B} \operatorname{grad} \varphi \quad \forall \varphi \in \mathcal{D}. \tag{15}$$

Hence, it is still reasonable to control a discrete divergence like (12) in the case of nonsmooth solutions.

The possible flux distributions of $\operatorname{div}^{(\star)}$ follow from conditions given in (9); see [33] for details. We obtain four possible flux distributions for cell $K$. Their support consists of only four cells. The nonvanishing values of the first flux distribution are given by

$$\begin{aligned} \hat{\Phi}^{(1)}_{i,j}\Big|_{i+1,j+1} &= (-\Delta x, \Delta y), & \hat{\Phi}^{(1)}_{i,j}\Big|_{i,j+1} &= (-\Delta x, -\Delta y), \\ \hat{\Phi}^{(1)}_{i,j}\Big|_{i,j} &= (\Delta x, -\Delta y), & \hat{\Phi}^{(1)}_{i,j}\Big|_{i+1,j} &= (\Delta x, \Delta y), \end{aligned} \tag{16}$$

and the others follow by translation as indicated in Figure 1. Note that the flux distributions are conservative in the sense of volume integrals, since the integral over the grid gives zero. From the flux distributions we conclude that the fluxes from one cell into another are no longer independent if we want to control the divergence. The sketch in Figure 1 demonstrates how the fluxes are coupled. A flux from $K$ into its right neighbor, i.e., a change of the magnetic flux density in that cell, immediately implies a flux into, e.g., the upper right corner. If this coupling is not respected, the divergence preservation is not guaranteed.

Thus, the update in a numerical method which is constraint preserving must be built out of linear combinations of flux distributions as in (16). Once such a scheme is constructed the local value of the discrete divergence operator $\operatorname{div}^{(\star)}$ in (12) will remain completely unchanged during the time steps. The values of the operator given by the discrete initial conditions will be exactly preserved.

**4.2. Identification of flux distributions.** Equipped with the information of the last section, we will now modify a generic finite volume scheme (see, e.g., [16]) for magnetohydrodynamics such that it becomes locally divergence preserving. It is sufficient to consider only the part of the scheme updating the magnetic flux density,

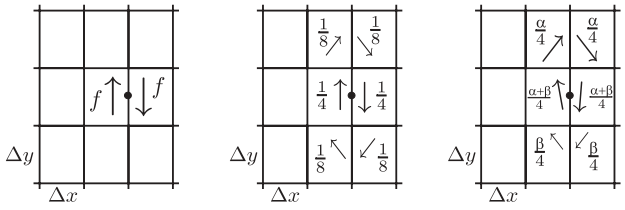


FIG. 2. *Left: The flux distribution attached to an edge in a classical finite volume scheme. This flux distribution is not divergence preserving. Middle and right: The modified flux distribution, which consists of the superposition of two flux distributions sketched in Figure* 1. *Hence, this flux distribution will preserve the discrete divergence* $\mathrm{div}^{(\star)}$.

given by

$$\mathbf{B}_{i,j}^{n+1} = \mathbf{B}_{i,j}^{n} + \frac{\Delta t}{\Delta x}(\mathbf{F}_{i-\frac{1}{2},j} - \mathbf{F}_{i+\frac{1}{2},j}) + \frac{\Delta t}{\Delta y}(\mathbf{G}_{i,j-\frac{1}{2}} - \mathbf{G}_{i,j+\frac{1}{2}}), \tag{17}$$

where $\mathbf{F}$ and $\mathbf{G}$ are magnetic field components of intercell fluxes, which are obtained for the full set of conservative variables. These intercell fluxes are assumed to be given by any Riemann solver (e.g., HLLE or Roe). These fluxes depend on *all* MHD variables on both sides of the edge under consideration. However, this dependency is suppressed in this and the following sections. Since the type of Riemann solver remains unspecified, the following modifications may be applied to virtually any finite volume scheme.

As a first step the flux distributions $\Phi^{(\mathrm{class})}$ of the classical scheme given in (17) are identified. Due to the curl-structure of the induction equation (2), the flux $\mathbf{F}$ in the $x$-direction changes only the $y$-component of the magnetic flux density, and vice versa for the flux $\mathbf{G}$. Furthermore, the amplitude of both intercell fluxes is given by a single scalar function $f$, and hence we write

$$\mathbf{F}_{i+\frac{1}{2},j} = -f_{i+\frac{1}{2},j} \begin{pmatrix} 0 \\ 1 \end{pmatrix} \qquad \text{and} \qquad \mathbf{G}_{i,j+\frac{1}{2}} = f_{i,j+\frac{1}{2}} \begin{pmatrix} 1 \\ 0 \end{pmatrix}. \tag{18}$$

The flux distributions are most easily defined when attached to the cell interfaces. The definition

$$\Phi^{(\mathrm{class})}_{i+\frac{1}{2},j}\Big|_{i,j} = f_{i+\frac{1}{2},j} \begin{pmatrix} 0 \\ \Delta y \end{pmatrix}, \qquad \Phi^{(\mathrm{class})}_{i+\frac{1}{2},j}\Big|_{i+1,j} = f_{i+\frac{1}{2},j} \begin{pmatrix} 0 \\ -\Delta y \end{pmatrix}, \tag{19}$$

$$\Phi^{(\mathrm{class})}_{i,j+\frac{1}{2}}\Big|_{i,j} = f_{i,j+\frac{1}{2}} \begin{pmatrix} -\Delta x \\ 0 \end{pmatrix}, \qquad \Phi^{(\mathrm{class})}_{i,j+\frac{1}{2}}\Big|_{i,j+1} = f_{i,j+\frac{1}{2}} \begin{pmatrix} \Delta x \\ 0 \end{pmatrix} \tag{20}$$

leads to the equivalent flux distribution formulation

$$\mathbf{B}_{i,j}^{n+1} = \mathbf{B}_{i,j}^{n} + \frac{\Delta t}{\Delta x \Delta y} \left( \Phi^{(\mathrm{class})}_{i+\frac{1}{2},j} + \Phi^{(\mathrm{class})}_{i-\frac{1}{2},j} + \Phi^{(\mathrm{class})}_{i,j+\frac{1}{2}} + \Phi^{(\mathrm{class})}_{i,j-\frac{1}{2}} \right)\Big|_{i,j} \tag{21}$$

of the scheme (17). So far nothing has happened except a reformulation of the finite volume scheme. One flux distribution of the classical scheme is depicted at the left-hand side of Figure 2. Note that the evaluation of the divergence on neighboring cells in the sense of (9) will not vanish using the operator $\mathrm{div}^{(0)}$ or $\mathrm{div}^{(\star)}$; hence, the classical scheme (17) does not preserve these divergence operators in general. Furthermore, if we consider the entire family of second-order 3×3 divergence operators given in [33],

none of these operators will be preserved in general. Still, the operators could be preserved in special situations like essentially one-dimensional grid aligned flows or due to lucky cancellations.

A divergence-preserving scheme may be established by modifying the flux distributions such that they form linear combinations of the flux distributions $\Phi_{i,j}^{(1,2,3,4)}$ given in the previous section. The difficulty lies in obtaining a consistent method. We suggest the use of

$$\Phi_{i+\frac{1}{2},j}^{(\mathrm{div})} = -\frac{1}{4} f_{i+\frac{1}{2},j} \left( \alpha \, \Phi_{i,j}^{(1)} + \beta \, \Phi_{i,j}^{(4)} \right) \tag{22}$$

as the divergence-preserving flux distribution. The coefficients $\alpha$ and $\beta$ are weighting coefficients which sum up to unity. The nonvanishing values of this distribution are given by

(23)

$$\begin{aligned}
\Phi_{i+\frac{1}{2},j}^{(\mathrm{div})}\Big|_{i,j+1} &= \frac{\alpha}{4} f_{i+\frac{1}{2},j} \begin{pmatrix} \Delta x \\ \Delta y \end{pmatrix}, & \Phi_{i+\frac{1}{2},j}^{(\mathrm{div})}\Big|_{i+1,j+1} &= \frac{\alpha}{4} f_{i+\frac{1}{2},j} \begin{pmatrix} \Delta x \\ -\Delta y \end{pmatrix}, \\
\Phi_{i+\frac{1}{2},j}^{(\mathrm{div})}\Big|_{i,j} &= \frac{1}{4} f_{i+\frac{1}{2},j} \begin{pmatrix} (\beta-\alpha)\Delta x \\ \Delta y \end{pmatrix}, & \Phi_{i+\frac{1}{2},j}^{(\mathrm{div})}\Big|_{i+1,j} &= \frac{1}{4} f_{i+\frac{1}{2},j} \begin{pmatrix} (\beta-\alpha)\Delta x \\ -\Delta y \end{pmatrix}, \\
\Phi_{i+\frac{1}{2},j}^{(\mathrm{div})}\Big|_{i,j+1} &= \frac{\beta}{4} f_{i+\frac{1}{2},j} \begin{pmatrix} -\Delta x \\ \Delta y \end{pmatrix}, & \Phi_{i+\frac{1}{2},j}^{(\mathrm{div})}\Big|_{i+1,j+1} &= \frac{\beta}{4} f_{i+\frac{1}{2},j} \begin{pmatrix} -\Delta x \\ -\Delta y \end{pmatrix},
\end{aligned}$$

and its sketch may be found on the right-hand side of Figure 2. The flux distribution $\Phi_{i,j+\frac{1}{2}}^{(\mathrm{div})}$ is built analogously with weights $\gamma$ and $\delta$. These flux distributions use the same amplitude of the intercell fluxes as the classical distribution except they distribute this flux on more cells. This larger support results in a more lengthy formulation of the scheme, since the value $\mathbf{B}_{i,j}^{n+1}$ is influenced by intercell fluxes of neighboring cells. The scheme with divergence-preserving flux distributions reads

$$\begin{aligned}
\mathbf{B}_{i,j}^{n+1} = \mathbf{B}_{i,j}^{n} &+ \frac{\Delta t}{\Delta x \Delta y} \left( \Phi_{i+\frac{1}{2},j}^{(\mathrm{div})} + \Phi_{i-\frac{1}{2},j}^{(\mathrm{div})} + \Phi_{i,j+\frac{1}{2}}^{(\mathrm{div})} + \Phi_{i,j-\frac{1}{2}}^{(\mathrm{div})} \right)\Big|_{i,j} \\
&+ \frac{\Delta t}{\Delta x \Delta y} \left( \Phi_{i+\frac{1}{2},j+1}^{(\mathrm{div})} + \Phi_{i-\frac{1}{2},j+1}^{(\mathrm{div})} + \Phi_{i+1,j+\frac{1}{2}}^{(\mathrm{div})} + \Phi_{i+1,j-\frac{1}{2}}^{(\mathrm{div})} \right)\Big|_{i,j} \\
&+ \frac{\Delta t}{\Delta x \Delta y} \left( \Phi_{i+\frac{1}{2},j-1}^{(\mathrm{div})} + \Phi_{i-\frac{1}{2},j-1}^{(\mathrm{div})} + \Phi_{i-1,j+\frac{1}{2}}^{(\mathrm{div})} + \Phi_{i-1,j-\frac{1}{2}}^{(\mathrm{div})} \right)\Big|_{i,j}.
\end{aligned} \tag{24}$$

This scheme is a conservative finite volume method, and hence approximation of the true weak solutions is assured by the Lax–Wendroff theorem. Obviously the new scheme has a larger stencil and is expected to introduce slightly more diffusion into the numerical solution. However, the extension of the stencil does not apply to the variables other than the magnetic field. Correspondingly, a decrease of resolution has not been observed in the numerical experiments; see also Figure 6. The shocks are smoothed out across the same number of cells. It is also important to note that preservation of the divergence requires the coupling of the changes in the neighboring cells and leads necessarily to a larger stencil. For the same reason the preserving scheme appears with a multidimensional flavor. It becomes evident that multidimensionality is a key issue in controlling the divergence constraint.

The weighting parameters $\alpha$ and $\beta$ have remained unspecified so far. They correspond to the weights used in [33] to activate different flux distributions in an advection

scheme. The special case $\alpha = \beta = \frac{1}{2}$ leads to a symmetric method. This method is equivalent to the staggered grid method of [4], where the intercell fluxes are utilized to update the edge centered values of $\mathbf{B}$. The equivalence becomes evident if the averaging formulas given in [34] for the staggered grid schemes are used. In [34] formulas similar to (26) and (27) may be found, but derived from *staggered grid schemes*. The formulas differ by some signs, but follow the same spirit of a direct finite volume update.

The freedom in the weights makes the present scheme more powerful, and we are able to incorporate additional upwinding into the scheme. One possibility is to consider an estimate of the fastest and slowest characteristic velocity in the $y$-direction, $\lambda_N^{(y)}$ and $\lambda_1^{(y)}$, at the interface $(i+\frac{1}{2}, j)$. The weights are then calculated by

$$\alpha = \frac{\left(\lambda_N^{(y)}\right)_+}{\left(\lambda_N^{(y)}\right)_+ + \left(-\lambda_1^{(y)}\right)_+}, \quad \beta = \frac{\left(-\lambda_1^{(y)}\right)_+}{\left(\lambda_N^{(y)}\right)_+ + \left(-\lambda_1^{(y)}\right)_+}, \tag{25}$$

where $(a)_+$ gives $\max(a, 0)$. Analogous expressions may be found for the edge $(i, j+\frac{1}{2})$ by considering the characteristics in the $x$-direction. This approach follows the ideas of [33], where the weighting is shown to be crucial for the stability of the scheme. In the case of a supersonic, i.e., superfast, MHD flow in the $y$-direction, we have either $\lambda_1, \lambda_N > 0 \Rightarrow \alpha = 1, \beta = 0$ or $\lambda_1, \lambda_N < 0 \Rightarrow \alpha = 0, \beta = 1$. Hence, only a single flux distribution in one of the corners, as shown in Figure 1, will be activated. This additional upwinding also reduces the stencil of the magnetic field update, which results in sharper resolution of superfast shock waves (see below). In [4] there is also an additional upwind weighting discussed in the case of a staggered grid method. However, the authors do not consider characteristic information for the weighting, but rather use gradient evaluations. Their ideas could also be incorporated into the present scheme to specify different weights $\alpha$ and $\beta$.

*Remark on the implementation.* The formulation through flux distributions is an auxiliary concept used in order to construct the preservation of the divergence and the conservation in the sense of volume integrals. In fact it is not needed for the implementation of the scheme. An existing finite volume scheme for magnetohydrodynamics may be modified appropriately by adding only a few lines. During the classical update (17) implemented by running through the edges, one has to identify the amplitudes $f_{i+\frac{1}{2},j}$ and $f_{i,j+\frac{1}{2}}$ from the intercell fluxes and to update the neighbors across the corners, as indicated in Figure 2 or in (23).

**4.2.1. Consistency.** To show the consistency of the divergence-preserving scheme, we first consider the case $\alpha = \beta = \gamma = \delta = \frac{1}{2}$ and make the flux distributions in (24) explicit. After rearranging the resulting terms, we obtain the equivalent formulation

$$\mathbf{B}_{i,j}^{n+1} = \mathbf{B}_{i,j}^{n} + \Delta t \begin{pmatrix} \frac{1}{\Delta y}(\langle f_{i,j-\frac{1}{2}} \rangle - \langle f_{i,j+\frac{1}{2}} \rangle) \\ \frac{1}{\Delta x}(\langle f_{i+\frac{1}{2},j} \rangle - \langle f_{i-\frac{1}{2},j} \rangle) \end{pmatrix}, \tag{26}$$

where the angular brackets stand for the averaging

$$\langle f_{i,j+\frac{1}{2}} \rangle = \frac{1}{8}(2f_{i,j+\frac{1}{2}} + f_{i+1,j+\frac{1}{2}} + f_{i-1,j+\frac{1}{2}} + f_{i-\frac{1}{2},j} + f_{i+\frac{1}{2},j} + f_{i-\frac{1}{2},j+1} + f_{i+\frac{1}{2},j-1}),$$
$$\langle f_{i+\frac{1}{2},j} \rangle = \frac{1}{8}(2f_{i+\frac{1}{2},j} + f_{i+\frac{1}{2},j+1} + f_{i+\frac{1}{2},j-1} + f_{i,j-\frac{1}{2}} + f_{i,j+\frac{1}{2}} + f_{i+1,j-\frac{1}{2}} + f_{i-1,j+\frac{1}{2}}) \tag{27}$$

of the neighboring intercell fluxes. Assuming that the intercell flux amplitudes $f_{i+\frac{1}{2},j}$ are at least second-order approximations to the exact values, e.g., by linear reconstruction, we proceed with a Taylor expansion of the above given scheme. Finally this leads to the statement

$$\begin{pmatrix} \frac{1}{\Delta y}(\langle f_{i,j-\frac{1}{2}}\rangle - \langle f_{i,j+\frac{1}{2}}\rangle) \\ \frac{1}{\Delta x}(\langle f_{i+\frac{1}{2},j}\rangle - \langle f_{i-\frac{1}{2},j}\rangle) \end{pmatrix} = \begin{pmatrix} -\partial_y f \\ \partial_x f \end{pmatrix}_{i,j} + \mathcal{O}(h^2), \tag{28}$$

which shows second-order consistency in space with the induction equation (2). Second order in time may now be obtained by Runge–Kutta integration of the residual.

The case of weights different from $\frac{1}{2}$ but constant in the grid may be considered analogously. However, in general, the weights are varying in the grid, and additional terms have to be included in (26) in order to obtain full second order; see also [33]. The elaboration of this issue remains for future work.

**4.3. Numerical examples.** In this section we investigate the capabilities of the new divergence-preserving scheme in comparison to the classical scheme by numerical experiments. Both schemes were implemented using linear reconstruction, dimensional Strang splitting, and Heun integration in time. Second-order consistency is shown by considering a smooth solution, while the divergence preservation is demonstrated using the discontinuous solutions of a Riemann problem. For all computations in this paper, the adiabatic coefficient was set to be $\gamma = \frac{5}{3}$, which represents the realistic case of a monatomic plasma.

**4.3.1. Empirical order of convergence.** For the empirical order of convergence, we consider the computational domain $[-1, 1]^2$ with periodic boundary conditions and the smooth initial conditions

$$\begin{aligned} \rho_0(x,y) &= \frac{3}{2} + \frac{1}{2}\sin(\pi x) + \frac{1}{4}\cos(\pi y), & p_0(x,y) &= \frac{1}{4}, \\ \mathbf{v}_0(x,y) &= \begin{pmatrix} 1 + \frac{1}{2}\sin(\pi y) + \frac{1}{4}\cos(\pi x) \\ 1 + \frac{1}{4}\sin(\pi x) + \frac{1}{2}\cos(\pi y) \end{pmatrix}, & \mathbf{B}_0(x,y) &= \begin{pmatrix} \frac{1}{2} \\ 1 \end{pmatrix}, \end{aligned} \tag{29}$$

with $v^{(z)} = B^{(z)} = 0$. Simulations with both the classical finite volume scheme (17) and the modified scheme (24) with symmetric weighting were conducted up to an end time $t = 0.2$. In both cases the intercell fluxes were obtained by use of the HLLE Riemann solver for magnetohydrodynamics as described, e.g., in [31] or [36]. The maximal Courant number was 0.9, and both schemes used an adaptive time step algorithm. The linear reconstruction was limited by the well-known weighted ENO (WENO) limiter [21]. In order to derive empirical orders of convergence, we calculate a reference solution on a fine grid (1200×1200 cells) with the divergence-preserving scheme. It is interesting to note that it was not possible to obtain a reference solution with the classical scheme. On grids with resolutions beyond 1000×1000 the classical scheme fails *due to divergence errors*. On very fine meshes these errors accumulate during the calculation, though the solution remains smooth. This failure is not present for the coarse grids considered in Figure 3. However, the failure illustrates how urgently a divergence control is needed for MHD calculations.

The errors of the magnetic energy $\frac{1}{2}\mathbf{B}^2$ compared to the reference solution are shown in Figure 3 for grids with resolutions up to 200×200. Both schemes, the classical and the divergence-preserving, exhibit second order for this problem. The errors of

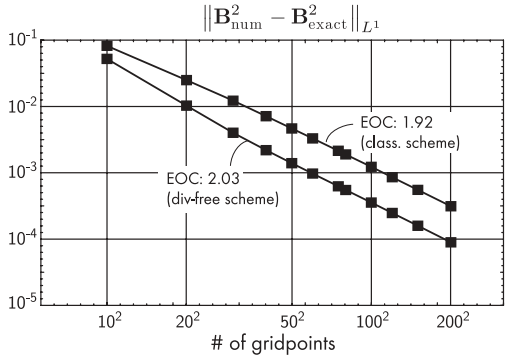


FIG. 3. *Comparison of the empirical order of convergence of the classical scheme and the modified divergence-preserving scheme. Both schemes attain second order. The plot shows only the error of the magnetic energy* $\frac{1}{2}\mathbf{B}^2$. *For the "exact" solution, a reference solution obtained on a* $1200 \times 1200$ *grid was used.*

the divergence-preserving schemes are smaller, which might also be explained by the fact that the reference solution was obtained by the divergence-preserving scheme as well. The second order is present in all fields of the MHD variables. The errors of all other variables, except those of the magnetic field, obtained with the classical and the divergence-free scheme are almost indistinguishable. Therefore we skip the presentation of these errors.

**4.3.2. Upwind weighting.** In order to present the capabilities of the upwind weighted scheme, we consider an MHD shock wave from the fast characteristic family in diagonal grid direction $(1,1)^T$. The acoustic Mach number of the inflow is chosen to be $M_0 = 4.5$, which corresponds to the Mach number of the shock. A diagonal velocity of $\mathbf{v} = 1.2$ is superposed such that the shock wave is not stationary but travels slowly across the grid. This setting can be interpreted as part of an evolving bow shock simulation.

Due to the superfast diagonal velocity, the weighting in (25) activates only the flux distribution $\Phi^{(1)}$ for both the $y$- and $x$-intercell flux. This results in a minimal stencil which still preserves the extended divergence operator $\text{div}^{(\star)}$ locally for every time step. The simulation is conducted on a $100 \times 100$ grid, and approximately 500 time steps are calculated. To focus on the effect of the weighting, the calculations did not use linear reconstruction, and the Strang splitting was substituted by simple additive splitting, which restricts the Courant number $\lesssim 0.5$. Figure 4 shows the shock profiles for the magnetic field components $B^{(x)}$ and $B^{(y)}$. Additionally, the plots show the results with the symmetric weights (larger stencil) and with the uncorrected, classical method. In the case of the classical method, divergence errors are created and the shock profile becomes oscillatory. The profile is resolved within 3–5 grid cells. In the upwind part of the profile, the weighted scheme shows a significant increase in resolution in comparison with the symmetrically weighted scheme.

**4.3.3. Riemann problem.** The control of the divergence becomes a most important issue if discontinuous solutions have to be calculated. Divergence errors occur at the discontinuities and contaminate the rest of the computational domain. In such cases it is also interesting to compare the different divergence operators given in the previous sections. As a test case we consider the two-dimensional Riemann problem

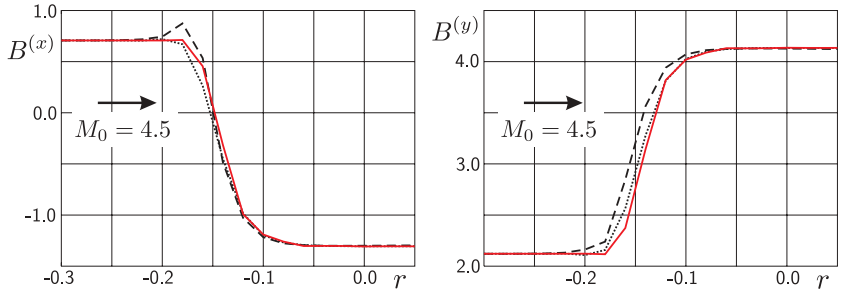


FIG. 4. *Plots of the magnetic flux density component $B^{(x)}$ (left) and $B^{(y)}$ (right) for a fast MHD shock wave traveling in diagonal grid direction with acoustic Mach number $M_0 = 4.5$. The solid line shows the result of the scheme with upwind weighted flux distributions (minimal stencil). The dotted line is obtained with the symmetric scheme. The result of the classical uncorrected scheme is shown with a dashed line. The upwind weighted scheme gives the best resolution of the shock.*

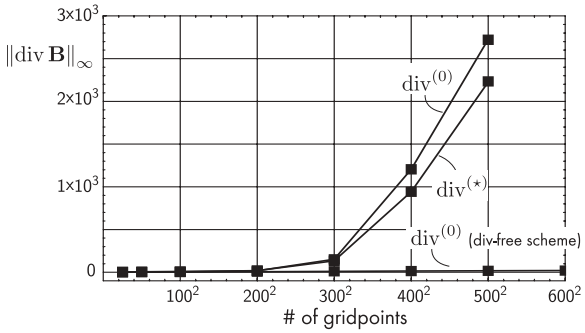


FIG. 5. *Behavior of the discrete divergence. The plot shows results for the classical (both upper curves) and the divergence-preserving (lower curve) schemes in the case of the Riemann problem given in* (30) *at time $t = 0.1$ on different grids. For the divergence-preserving scheme, the operator $\mathrm{div}^{(\star)}$ gives exactly zero, while $\mathrm{div}^{(0)}$ grows very slowly if the grid is refined. For the classical scheme, evaluations of both operators explode and the calculation fails to reach $t = 0.1$ on grids larger than $500 \times 500$.*

given by the initial conditions

$$\rho_0(x,y) = \begin{cases} 10 & x<0,\ y<0, \\ 1 & \text{else}, \end{cases} \qquad p_0(x,y) = \begin{cases} 15 & x<0,\ y<0, \\ \frac{1}{2} & \text{else}, \end{cases} \tag{30}$$

with $\mathbf{B}_0 = 1/\sqrt{2}(1,\ 1,\ 0)^T$ and $\mathbf{v}_0 \equiv 0$. The computational domain was chosen to be $[-0.4, 0.4]^2$ and the end time is $t = 0.1$. Again, we used $CFL = 0.9$ and an adaptive time step. The boundaries are extended with ghost cells filled with constant extrapolation of the values of the inner cells.

We calculated the problem with the classical scheme and the new divergence-preserving scheme for different grid resolutions. Once $t = 0.1$ has been reached, the discrete divergence is evaluated using the classical operator (11) and the extended operator (12). The infinity norm of these evaluations is depicted in Figure 5 for the different grids. As expected, the divergence of the classical scheme grows rapidly independent of the operator. Furthermore, this growth yields a failure of the scheme at high resolutions.

In the calculation with the divergence-preserving scheme, the evaluation of $\mathrm{div}^{(\star)}$

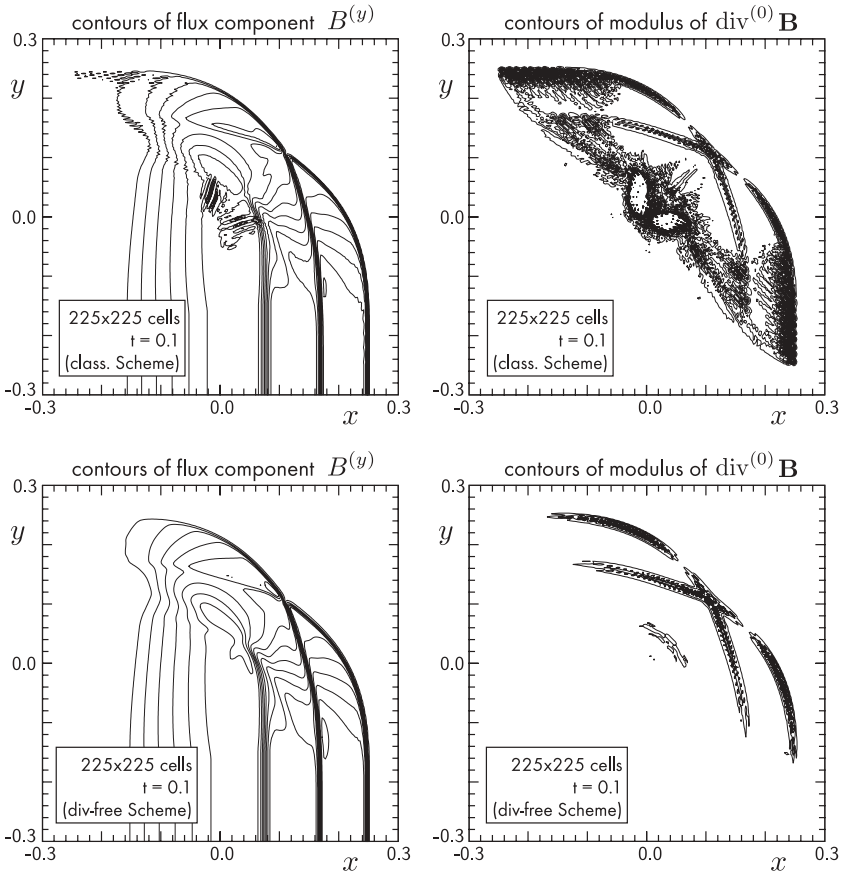


FIG. 6. *Comparison of the classical (top) and the modified divergence-free (bottom) schemes in the case of the Riemann problem* (30) *on a rectangular grid at* $t = 0.1$. *The figure shows the contours of the magnetic flux component* $B^{(y)}$ *and of the classical discrete divergence* $\mathrm{div}^{(0)}$. *The extended divergence* $\mathrm{div}^{(\star)}$ *gives exactly zero in the case of the divergence-free scheme and a similar plot as* $\mathrm{div}^{(0)}$ *for the classical scheme. The calculation with the classical scheme fails at higher resolutions.*

gives zero for the entire calculation in accordance with the theoretical result that this operator is exactly preserved. The operator $\mathrm{div}^{(0)}$, however, gives nonvanishing results due to the discontinuities present in the solution. This will be discussed in the following paragraphs.

Figure 6 shows the result of the Riemann problem at $t = 0.1$ obtained with $300\times300$ cells. Note that the number of cells given in the figure corresponds to the reduced domain which is shown. Besides the contours of $B^{(y)}$ the figure shows the contours of the absolute value of $\mathrm{div}^{(0)}\,\mathbf{B}$ for the classical (upper row) and the new divergence-free (lower row) schemes. The divergence is significantly disturbed when using the classical scheme, resulting in a nonphysical solution of $B^{(y)}$ and also of all other variables due to the coupling of the equations.

The divergence-preserving scheme gives a clearly resolved solution for the magnetic flux density $B^{(y)}$. Furthermore, the operator $\mathrm{div}^{(0)}$ gives a nonvanishing value only in the vicinity of oblique shocks. This represents the fact that the classical operator differs from the extended operator by some cross derivatives as given in (14). In

smooth domains of the solutions, these cross derivatives are finite and give rise only to a second-order difference between the classical and the extended operator, which is exactly zero. Additionally, these cross derivatives vanish in the case of coordinate aligned and diagonal shocks, and in these cases the preservation of the extended operators entails a vanishing classical operator. This is also visible in Figure 6. However, in oblique shocks these cross derivatives become large; hence, $\operatorname{div}^{(0)}$ will give a finite value. The plot in Figure 6 demonstrates that these values stay attached to the shocks and in the limit the operator $\operatorname{div}^{(0)}$ will give zero almost everywhere. At the resolution $500\times500$ ($\Delta x = 0.0016$) the maximal value of the classical operator is $\operatorname{div}^{(0)} \mathbf{B} \approx 14$. By comparison with the residual expression in (14), this value shows that the cross derivatives have an order of magnitude $O(\Delta x^{-2})$, resulting in a finite value of $\operatorname{div}^{(0)} \mathbf{B}$.

**5. Triangular grids.** The construction of locally divergence-preserving schemes is not restricted to rectangular grids. This section considers triangular grids. The goal is to construct constraint-preserving methods on triangular grids in a way analogous to that of the previous section. We will use the results of the rectangular case and give an appropriate divergence operator and the according flux distribution directly. This yields a scheme completely analogous to the rectangular case. In the next section an alternative deduction of the preserving methods is presented which will provide additional understanding of the presented methods.

The triangular grid consists of vertices $p_i$ which combine into triangles or cells, e.g., $K_{i,j,k}$ built from $p_i$, $p_j$, and $p_k$. For the barycenter of cell $K$ we write $\mathbf{c}_K$. The cell $K_{i,j,k}$ is bounded by oriented edges $\mathbf{e}_{i,j}$, $\mathbf{e}_{j,k}$, and $\mathbf{e}_{k,i}$, ordered following a positive orientation of the boundary of the cell. The edge $\mathbf{e}_{i,j}$ points from vertex $p_i$ to $p_j$. The neighboring cell to the right of the edge $\mathbf{e}_{i,j}$ is denoted by $N_{i,j}$. For accuracy considerations we refer to $h = \max_K \operatorname{diam} K$. Finally, it is convenient to introduce the notation $(x, y)^\perp = (y, -x)$ for the orthogonal counterpart of a two-dimensional vector. Similar to the rectangular case, we will consider only inner cells and use ghost cells in the numerical experiments.

**5.1. Discrete divergence operators.** As in the rectangular case our first task is to look for discrete divergence operators on triangular grids. If we consider only the direct neighbors of a triangle (neighbors joining a common edge), the triangular grid leaves only a little freedom in constructing divergence operators. The only consistent operator which takes into account only the three direct neighbors of a cell is given by

$$\operatorname{div}^{(0)} \mathbf{B}\Big|_{K_{i,j,k}} \approx \frac{\mathbf{B}_{N_{j,k}} \cdot (\mathbf{c}_{N_{i,j}} - \mathbf{c}_{N_{k,i}})^\perp + \mathbf{B}_{N_{k,i}} \cdot (\mathbf{c}_{N_{j,k}} - \mathbf{c}_{N_{i,j}})^\perp + \mathbf{B}_{N_{i,j}} \cdot (\mathbf{c}_{N_{k,i}} - \mathbf{c}_{N_{j,k}})^\perp}{\frac{1}{2}(\mathbf{c}_{N_{j,k}} - \mathbf{c}_{N_{i,j}}) \cdot (\mathbf{c}_{N_{k,i}} - \mathbf{c}_{N_{i,j}})^\perp}, \tag{31}$$

which follows by requiring first-order consistency with the divergence in the barycenter of $K_{i,j,k}$. A second-order operator which uses only the direct neighbors of a general triangular cell does not exist since there is not enough freedom for eliminating the coefficients in the Taylor expansion. The rigorous evaluation of the generic statement (9) in order to obtain flux distributions for (31) is very difficult for a general triangular grid. Several flux distributions with different shapes have been assumed and tested by evaluation of the operator (31). None of the flux distributions turned out to be divergence preserving. It could well be that the operator (31) does not permit any sufficiently local flux distributions.

If we consider divergence operators which take into account all neighbors of a cell (also across a vertex), there is much more freedom for divergence approximations than in the rectangular case. Again, the construction and analysis of a general class of operators is very complicated. Instead, we construct a divergence operator which evaluates all neighboring cells, as the extended operator does for the rectangular case (12). This operator for a triangle may be written as

$$\operatorname{div}^{(\star)} \mathbf{B}\Big|_{K_{i,j,k}} = \frac{1}{3}\left(\operatorname{div}^{(\times)} \mathbf{B}\Big|_i + \operatorname{div}^{(\times)} \mathbf{B}\Big|_j + \operatorname{div}^{(\times)} \mathbf{B}\Big|_k\right) \tag{32}$$

using three evaluations of the divergence at the vertices of $K_{i,j,k}$ given by

$$\operatorname{div}^{(\times)} \mathbf{B}\Big|_i = \frac{3}{2} \frac{\sum\limits_{\text{all adjacent } K_{i,l,m}} \mathbf{B}_{K_{i,l,m}} \cdot \mathbf{e}_{l,m}^{\perp}}{\sum\limits_{\text{all adjacent } K_{i,l,m}} |K_{i,l,m}|}. \tag{33}$$

Using Taylor expansion the operator (32) can be shown to be first-order consistent with the divergence of $\mathbf{B}$ in the barycenter of $K_{i,j,k}$. Note that the rectangular operator $\operatorname{div}^{(\star)}$ can be written using (similar to (32), (33)) an averaging of divergence operators located in the vertices.

Surprisingly, neither (31) nor (32) is used in other works on divergence controlling on triangular grids. The authors of [10] use the operator

$$\operatorname{div}^{(+)} \mathbf{B}\Big|_{K_{i,j,k}} = \frac{\mathbf{B}_{N_{i,j}} \cdot \mathbf{e}_{i,j}^{\perp} + \mathbf{B}_{N_{j,k}} \cdot \mathbf{e}_{j,k}^{\perp} + \mathbf{B}_{N_{k,i}} \cdot \mathbf{e}_{k,i}^{\perp}}{|K_{i,j,k}|}, \tag{34}$$

which is consistent *only if* all triangles have the same edge-lengths. Indeed on arbitrary grids this operator does not show pointwise convergence to the exact divergence. Essentially, the operator (34) measures the jump of the normal components of the magnetic field across edges.

For a divergence-preserving scheme on triangular grids, we will consider the operator (32). It provides flux distributions which are equivalent to the flux distribution of the rectangular case. The aim is to construct flux distributions $\Phi_i$ that give exactly zero for (32). In the construction we do not follow the generic statement (9), which would be too cumbersome. We rather use the rectangular result and try to find analogous flux distributions that bend around a vertex; see Figure 1. Promising candidates may then easily be tested by application of the operator (32). In that way we obtain flux distributions that are attached to vertices, and their support consists of all cells around that vertex. Two of these flux distributions are depicted in Figure 7. Evaluation of the flux distribution in one of the adjacent cells gives

$$\Phi_i|_{K_{i,j,k}} = \frac{\mathbf{e}_{j,k}}{|K_{i,j,k}|}. \tag{35}$$

The application of the operator (33) to such a flux distribution vanishes for *any* vertex; hence the evaluation of the operator (32) will give zero in any cell. This establishes the condition (9) needed for divergence preservation. The vanishing of (33) for these flux distributions becomes clear by use of the relation $\mathbf{e}_{i,j}^{\perp} \cdot \mathbf{e}_{k,j} = 2\,|K_{i,j,k}|$ in the evaluation.

Note that the flux distribution in (35) is built such that the normal component across edges is constant, a property not shared by the rectangular flux distribution.

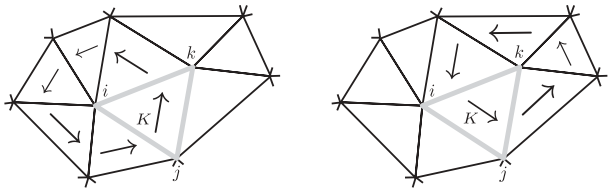


FIG. 7. *Sketches of two possible flux distributions that preserves the discrete divergence* $\operatorname{div}^{(\star)}$ *in case of a triangular grid. In each flux distribution the jump of the normal component between adjacent cells vanishes. Note the optical similarity with the flux distributions in the rectangular case. Again the flux distributions approximate closed curves according to a divergence-free field.*

This property represents the solenoidality in a weak sense. Furthermore, the evaluation of the operator (34) applied to the flux distribution (35) gives zero for all cells as well.

As in the rectangular case a numerical scheme built with the flux distributions $\Phi_i$ will exactly preserve the local values of $\operatorname{div}^{(\star)} \mathbf{B}$, and the classical operator (31) will not be preserved. However, since both operators $\operatorname{div}^{(\star)}$ and $\operatorname{div}^{(0)}$ are consistent, the operator $\operatorname{div}^{(0)}$ will stay bounded in any smooth region of the solution. According to the last paragraph, it will also exactly preserve the local values of $\operatorname{div}^{(+)} \mathbf{B}$, and it will not affect the jumps in the normal components across edges. That is, the scheme will not introduce additional jumps but preserve the jumps given by the initial conditions. This additional preservation property is restricted to triangular grids.

**5.2. Identification of flux distributions.** Knowledge of the possible flux distributions enables us to construct a divergence-preserving finite volume scheme. A finite volume update for the magnetic flux density on triangles is written in the form (see, e.g., [32])

$$\mathbf{B}^{n+1}_{K_{i,j,k}} = \mathbf{B}^{n}_{K_{i,j,k}} - \frac{\Delta t}{|K_{i,j,k}|} \sum_{\substack{l,m \text{ edge} \\ \text{of } K_{i,j,k}}} |\mathbf{e}_{l,m}| \; \mathcal{H}\left(\mathbf{B}^{n}_{K_{i,j,k}}, \mathbf{B}^{n}_{N_{l,m}}, \mathbf{e}_{l,m}\right), \tag{36}$$

where $\mathcal{H}(\mathbf{B}_K, \mathbf{B}_N, \mathbf{e})$ gives the magnetic part of the intercell flux across an edge $\mathbf{e}$. This intercell flux can be obtained by any Riemann solver and is here assumed to be given. The dependency of $\mathcal{H}$ on the other conservative variables is suppressed in (36). From the curl-structure of the induction equation in (2) it becomes evident that the amplitude of the flux $\mathcal{H}$ is given by a single scalar function $f$, while its direction is always parallel to the edge under consideration. Hence, if we define a flux distribution $\Phi^{(\text{class})}_{i,k}$ attached to the edge $\mathbf{e}_{i,k}$ by

$$\Phi^{(\text{class})}_{i,k}\Big|_{K_{i,j,k}} = f_{i,k} \frac{\mathbf{e}_{k,i}}{|K_{i,j,k}|}, \qquad \Phi^{(\text{class})}_{i,k}\Big|_{K_{i,k,l}} = f_{i,k} \frac{\mathbf{e}_{i,k}}{|K_{i,k,l}|}, \tag{37}$$

then the classical scheme (36) has the form

$$\mathbf{B}^{n+1}_{K_{i,j,k}} = \mathbf{B}^{n}_{K_{i,j,k}} + \Delta t \left(\Phi^{(\text{class})}_{i,j} + \Phi^{(\text{class})}_{j,k} + \Phi^{(\text{class})}_{k,i}\right)\Big|_{K_{i,j,k}}. \tag{38}$$

Here, $f_{i,k}$ gives the amplitude (possibly negative) of the intercell flux through edge $\mathbf{e}_{i,k}$ from left to right. The left-hand side of Figure 8 shows the shape of the flux distribution $\Phi^{(\text{class})}_{i,k}$ for a positive $f_{i,k}$. As in the rectangular case this flux distribution

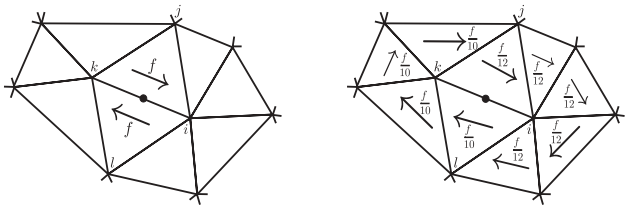


FIG. 8. *Left: The flux distribution of a classical finite volume scheme for the induction equation. The discrete divergence is not preserved. Right: The flux distribution of the new divergence-free scheme which results from superposition of two flux distributions around vertex i and k. The vectors in $K_{i,j,k}$ and $K_{i,k,l}$ follow from the average in* (39).

does not preserve any discrete divergence operator. Following the ideas of the previous section, we modify the flux distribution such that it becomes a linear combination of the $\Phi_i$'s given in (35) and Figure 7.

The definition

$$\Phi_{i,k}^{(\mathrm{div})} = \frac{1}{2}\left(\frac{f_{i,k}}{\#p_i}\Phi_i + \frac{f_{i,k}}{\#p_k}\Phi_k\right) \tag{39}$$

gives a flux distribution as shown on the right-hand side of Figure 8. The symbol $\#p_i$ denotes the number of edges emerging from the vertex $p_i$. Obviously this flux distribution is divergence preserving since it is a linear combination of divergence-preserving flux distributions. As in the rectangular case it is possible to weight the flux distributions differently. Here, we restrict ourselves to the symmetric scheme. Note that the values of $\Phi_{i,k}^{(\mathrm{div})}$ in $K_{i,j,k}$ and $K_{i,k,l}$ are not parallel to $\mathbf{e}_{i,k}$ if $\#p_i \neq \#p_k$ as indicated in the sketch of Figure 8. In the resulting scheme the magnetic flux density in one cell is not only influenced by the direct neighbors but also by neighbors across vertices. The scheme reads

$$\mathbf{B}_{K_{i,j,k}}^{n+1} = \mathbf{B}_{K_{i,j,k}}^{n} + \Delta t\left(\Phi_{i,j}^{(\mathrm{div})} + \Phi_{j,k}^{(\mathrm{div})} + \Phi_{k,i}^{(\mathrm{div})}\right)\Big|_{K_{i,j,k}} + \Delta t \sum_{\substack{l \text{ or } m \\ \in (i,j,k)}} \Phi_{l,m}^{(\mathrm{div})}\Big|_{K_{i,j,k}}. \tag{40}$$

In analogy to the method on rectangular grids, this scheme is a conservative finite volume method. It possesses a larger stencil to account for the control of the discrete divergence.

*Remark on the implementation.* Again the formulation with flux distributions is not necessary in the implementation. A finite volume program which runs through all edges updating the neighboring cells with the intercell flux may easily be modified. Once the amplitude $f$ is obtained from the intercell flux, this flux has to be distributed to all neighbors sharing the same vertices as the edge (see Figure 8 right).

**5.2.1. Consistency.** Taylor expansion of the classical finite volume scheme (38) leads to

$$\begin{aligned}\left(\Phi_{i,j}^{(\mathrm{class})} + \Phi_{j,k}^{(\mathrm{class})} + \Phi_{k,i}^{(\mathrm{class})}\right)\Big|_{K_{i,j,k}} &= \frac{f_{i,j}\,\mathbf{e}_{i,j} + f_{j,k}\,\mathbf{e}_{j,k} + f_{k,i}\,\mathbf{e}_{k,i}}{|K_{i,j,k}|} \\ &= \begin{pmatrix} -\partial_y f \\ \partial_x f \end{pmatrix}_{K_{i,j,k}} + \mathcal{O}(h)\end{aligned} \tag{41}$$

if the approximations of the intercell fluxes $f$ are assumed to be at least first order. The same assumption and some rearranging of the expressions in the divergence-preserving scheme (40) yields the similar statement

$$\begin{aligned}
&\left(\Phi^{(\mathrm{div})}_{i,j} + \Phi^{(\mathrm{div})}_{j,k} + \Phi^{(\mathrm{div})}_{k,i}\right)\Big|_{K_{i,j,k}} + \sum_{l \text{ or } m \in (i,j,k)} \Phi^{(\mathrm{div})}_{l,m}\Big|_{K_{i,j,k}} \\
&= \frac{\langle f_{i,j} \rangle \mathbf{e}_{i,j} + \langle f_{j,k} \rangle \mathbf{e}_{j,k} + \langle f_{k,i} \rangle \mathbf{e}_{k,i}}{|K_{i,j,k}|} \\
&= \begin{pmatrix} -\partial_y f \\ \partial_x f \end{pmatrix}_{K_{i,j,k}} + \mathcal{O}(h). \qquad (42)
\end{aligned}$$

Here the averages of neighboring intercell fluxes

$$\langle f_{i,j} \rangle = \frac{1}{2}\left(\sum_{\substack{\text{edges } i,k \\ \text{around } p_i}} \frac{f_{i,k}}{\#p_i} + \sum_{\substack{\text{edges } l,j \\ \text{around } p_j}} \frac{f_{l,j}}{\#p_j}\right) \qquad (43)$$

arise, which have the same structure as the averages used in (27) in the rectangular case. Indeed, if (43) is evaluated for edges in a rectangular grid instead of a triangular one, we obtain exactly (27) after renaming the intercell fluxes. This completes the analogy of both the rectangular and triangular schemes.

Usually, classical methods on unstructured grids like in (36) are extended formally to second order by linear reconstruction and Runge–Kutta integration in time; see, e.g., [32], [36]. The divergence-preserving flux modification given in (40) is perfectly adapt to such a setting, since it uses the intercell fluxes directly. Furthermore, a Runge–Kutta integration may be viewed as successive evaluations of Euler time steps like in (40); hence the divergence will be preserved at every stage and in the final update.

**5.3. Numerical example.** Both schemes, the classical (36) and the divergence-preserving (40), have been implemented to examine test cases. As in the rectangular case the well-known HLLE flux, as described in [31] or [36] for magnetohydrodynamics, has been used to calculate the intercell fluxes. The implementation is restricted to first order for implementational convenience and purely designed to demonstrate the divergence preservation. However, the scheme (40) is expected to work as well for second order obtained by linear reconstruction and Runge–Kutta integration. Future work includes the incorporation of the modifications into existing codes, as in [10], as well as the comparison of the present modifications to other approaches of divergence corrections.

The Riemann problem given by (30) is considered as a test example. Here, we use the end time $t = 0.3$ and the computational domain $[-1, 1]^2$ covered by an unstructured triangular mesh. At the edges of the boundary of the domain the fluxes are obtained from the solution of a Riemann problem with the same values for the left- and right-hand states which corresponds to the use of zero-order extrapolated ghost cells. The mesh was generated using the routines of "pdetool" provided in MATLAB. The mesh was obtained first by generating a mesh with prescribed maximal edge-length and two successive regular and uniform refinements, yielding 105,568 triangles with a maximal edge-length $\approx 0.001$. The grid was unstructured both regarding the shape of the cells and the number of cells around a vertex. The implementation of the scheme was done in plain C.

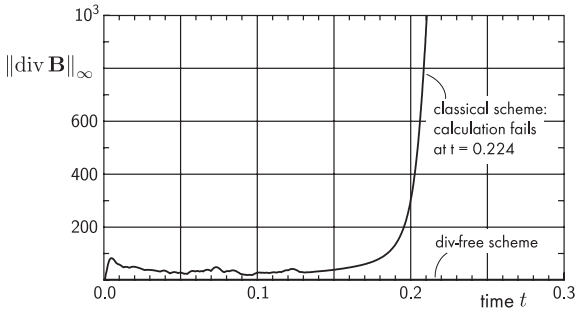


FIG. 9. *Time evolution of the discrete divergence* $\mathrm{div}^{(\star)}$ *in the Riemann problem* (30) *in the case of the classical and the divergence-preserving schemes on a unstructured grid with* 105,568 *cells. For the classical scheme the divergence grows in an uncontrolled manner, and the scheme stops at* $t = 0.224$ *due to a vanishing time step. Depending on the resolution and structure of the mesh, the failure occurs at different times. For the divergence-preserving scheme the discrete divergence vanishes for all times and coincides with the coordinate axis.*

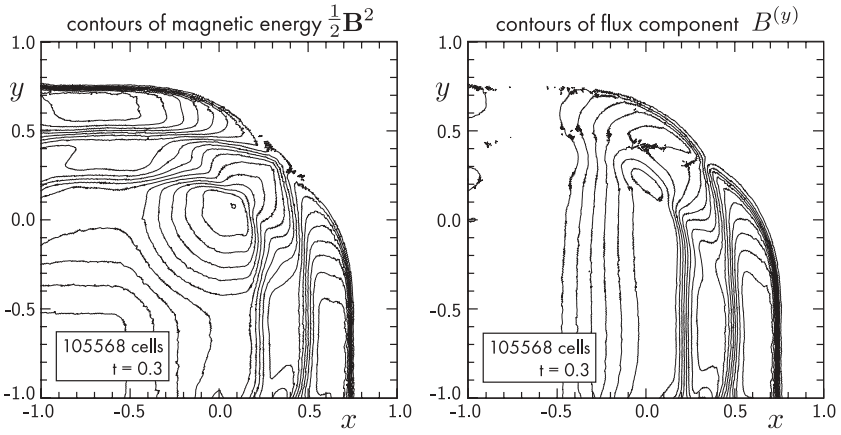


FIG. 10. *Contours of the magnetic energy* $\frac{1}{2}\mathbf{B}^2$ *and the magnetic flux component* $B^{(y)}$ *for the Riemann problem* (30) *at* $t = 0.3$. *The contours are spoiled from a poor boundary procedure but are free from divergence errors.*

Figure 9 shows the time evolution of the divergence operator (32) during the calculation with the classical and the divergence-preserving schemes. Initially this operator gives exactly zero in every cell. Only for the divergence-preserving scheme does this hold also for the entire calculation. In contrast, the divergence grows exponentially with time for the classical scheme, as can be seen in Figure 9. Indeed, the classical calculation fails before the calculation reaches the end time $t = 0.3$. As expected, it follows that a divergence control is mandatory for such a calculation.

The results for the Riemann problem (30) calculated with the divergence-preserving method are depicted in Figure 10. The figure shows the contours of the magnetic energy $\frac{1}{2}\mathbf{B}^2$ and of the magnetic flux density component $B^{(y)}$ at time $t = 0.3$. Note the self-similarity of the problem, which becomes apparent by comparison to Figure 6, where the result for $t = 0.1$ is shown. The plots in Figure 10 show less resolution of the discontinuities due to the first-order scheme. The calculation suffers from errors due to a poor boundary procedure for the fluxes. However, the calculation stays free of divergence errors.

**6. Alternative construction.** The finite volume methods of the previous sections were constructed by constraining their fluxes to preserve certain divergence operators from the very beginning. In the following we will present an alternative construction based on a finite element representation of the residual. Both ways provide different insights into the properties of the schemes. The following approach was inspired by the work [11]. A very recent paper [3] considers a similar approach in the context of staggered grids.

**6.1. Stokes formulation.** No doubt, the system of magnetohydrodynamics (1) is built from conservation laws, and only a conservative method based on fluxes will give reliable numerical approximations. Such schemes consider cell volume averages of the conservative variables. However, unlike the balance equations of mass, momentum, and energy, the weak formulation of the induction equation (2) is more naturally formulated on surfaces rather than in volumes.

The Stokes formulation in three dimensions is given by

$$\frac{d}{dt}\frac{1}{|\mathbf{A}|}\int_{\mathbf{A}} \mathbf{B}\cdot d\mathbf{A} = -\frac{1}{|\mathbf{A}|}\int_{\mathbf{A}} \operatorname{curl}\mathbf{B}\times\mathbf{v}\cdot d\mathbf{A} = -\frac{1}{|\mathbf{A}|}\int_{\partial\mathbf{A}} \mathbf{B}\times\mathbf{v}\cdot d\mathbf{e}, \tag{44}$$

which represents an evolution equation for a surface average of the magnetic flux density $\mathbf{B}$. Note that the preservation of the divergence follows immediately in the form

$$\frac{d}{dt}\frac{1}{|\mathbf{A}|}\oint_{\mathbf{A}} \mathbf{B}\cdot d\mathbf{A} = 0, \tag{45}$$

since a closed surface has no boundary. In the following subsections we construct a numerical method by approximating the evolution equation (44), which, however, must be linked to a finite volume approach of the other equations in the MHD system (1). As in the previous sections we restrict ourself to the two-dimensional case in which (44) reduces to

$$\frac{d}{dt}\frac{1}{|\mathbf{e}|}\int_{\mathbf{e}} \mathbf{B}\cdot d\mathbf{e}^{\perp} = -\frac{1}{|\mathbf{e}|}\,[\,f\,]_0^1 \tag{46}$$

for line segments. Hereafter, all vectors are two-dimensional, and $f$ is given by (4).

The basic approximation considers (46) for edges of cells of the computational domain. At first these cells shall be arbitrary polygons. The edge average on the left-hand side of (46) gives a mean normal component $\overline{b_{\mathbf{e}}}$ of the edge under consideration. The evolution equation then reads

$$\frac{d}{dt}\,\overline{b_{\mathbf{e}_{i,j}}} = -\frac{f_j - f_i}{|\mathbf{e}_{i,j}|} \tag{47}$$

for an edge $\mathbf{e}_{i,j}$ pointing from vertex $p_i$ to $p_j$. Here, the divergence preservation is automatically incorporated since the integral of the mean normal components around a cell border will remain constant. We have

$$\frac{d}{dt}\sum_{\substack{\mathbf{e}_{i,j}^{(K)}\ \text{edges}\\ \text{around } K}} \left|\mathbf{e}_{i,j}^{(K)}\right| \overline{b_{\mathbf{e}_{i,j}^{(K)}}} = 0; \tag{48}$$

hence, the residual in (47) is divergence preserving. The method in (47) is related to the correction scheme used in [4], [8], and [13] on a staggered grid to provide a solenoidal magnetic flux density on rectangular grids.

**6.2. Face elements.** In order to incorporate (47) into a finite volume approach, where cell averages play the major role, we only need to project the edge normal components to cell averages. This was also pointed out by De Sterck in [11]. We proceed by elaborating his approach.

De Sterck proposes using face elements, also called Nedelec elements [28], for this projection. These elements are well known in the finite element simulations of electrodynamics; see, e.g., [22], [6]. Face elements are basis functions that combine given mean normal components on the faces of a cell to a linear reconstruction of the field inside the cell. They are suited for the evolution of the mean fluxes across faces in (44). In two dimensions the reconstruction of a generic field $\Psi$ reads

$$\Psi|_K(\mathbf{x}) = \sum_{\text{edges of } K} \overline{\psi_{\mathbf{e}_{i,j}}}\, \mathbf{W}_K^{\mathbf{e}_{i,j}}(\mathbf{x}), \tag{49}$$

where $\mathbf{W}_K^{\mathbf{e}_{i,j}}$ are the face element. They are suited for the evolution (47). In two dimensions the face elements are attached to the edges as degenerate faces and correspond to Raviart–Thomas elements. The property of $\mathbf{W}_K^{\mathbf{e}_{i,j}}$ justifying the reconstruction in (49) is

$$\mathbf{e}_{k,l}^{\perp} \cdot \mathbf{W}^{\mathbf{e}_{i,j}}(\mathbf{x})|_{\mathbf{e}_{k,l}} = \begin{cases} |\mathbf{e}_{k,l}| & \text{if } \mathbf{e}_{k,l} = \mathbf{e}_{i,j}, \\ 0 & \text{other edges;} \end{cases} \tag{50}$$

that is, taking the mean normal component along an edge in (49) will yield an identity. The symbol $()^{\perp}$ again denotes the orthogonal counterpart. Furthermore, the normal component of the reconstructed function is constant along the edge, at least in the triangular and rectangular cases. For more properties, see [22] or other textbooks on finite elements. Face elements may be constructed for triangles and quadrilaterals in two dimensions and for tetrahedrons and hexahedrons in three dimensions.

Since the normal components on the edges are reproduced in (49), the reconstruction of the field of the entire computational domain will give a piecewise linear function with continuous normal components across cells. Additionally, we have

$$\sum_{\text{edges of } K} \overline{\psi_{\mathbf{e}_{i,j}}}\, |\mathbf{e}_{i,j}| = 0 \quad \text{in } K \quad \Rightarrow \quad \operatorname{div} \Psi = 0 \quad \text{in } K; \tag{51}$$

that is, if the closed integral of the given mean normal components on the boundary of a cell gives zero, the reconstructed field in this cell will be solenoidal. This property predestinates face elements for the reconstruction of fields given by the right-hand side of (47).

**6.3. Averaging.**

**6.3.1. General approach.** Since we are only interested in cell averages, each face element is integrated to give its cell average

$$\overline{\mathbf{W}_K^{\mathbf{e}_{i,j}}} := \frac{1}{|K|} \int_K \mathbf{W}_K^{\mathbf{e}_{i,j}}(\mathbf{x})\, d\mathbf{x}. \tag{52}$$

Using this averaged face element, we average the reconstruction (49) to obtain

$$\overline{\Psi_K} = \sum_{\text{edges of } K} \overline{\psi_{\mathbf{e}_{i,j}}}\, \overline{\mathbf{W}_K^{\mathbf{e}_{i,j}}} \tag{53}$$

for a generic field $\Psi$. This averaging using Nedelec reconstruction is called *Nedelec averaging* in what follows. It represents the required projection, which turns the evolution equation (47) into an equation for cell averages, that is,

$$\partial_t \overline{\mathbf{B}_K} = \sum_{\text{edges of } K} \frac{f_i - f_j}{|\mathbf{e}_{i,j}|} \overline{\mathbf{W}_K^{\mathbf{e}_{i,j}}}, \tag{54}$$

where $\overline{\mathbf{B}_K}$ is the cell average of the magnetic flux density. As mentioned earlier in this paper, the divergence-preserving property is needed primarily for the residual of the evolution equation. It is the residual which has to be solenoidal in order to provide a divergence-preserving update. The vanishing divergence of the magnetic flux density does not play a major role. Indeed, if the left-hand side in (54) was not divergence-free, e.g., an electric field, we still would need to proceed the same way since it is the curl-character of the residual which has to be matched.

It remains to specify the evaluations of the function $f$ given by (4) at the vertices in (54). In [11] this had been done by a residual distribution scheme. Here, we will try to stay close to a finite volume approach for the entire MHD system (1). In order to use the information obtained by intercell fluxes, we define

$$f_i = \sum_{\substack{\text{edges } i,j \\ \text{around } p_i}} \frac{f_{i,j}}{\#p_i} \tag{55}$$

for the vertex evaluations. As in the previous sections $f_{i,j}$ is the amplitude of the magnetic intercell flux and $\#p_i$ gives the number of edges at vertex $p_i$. This definition will become more justified in the following two subsections. There, it yields numerical methods equivalent to the symmetrically weighted schemes given before in (24) and (40), which were constructed directly upon modifications of the intercell flux. One may think of some weighted definition for $f_i$ which will result in weighted schemes. In [11] a residual distribution scheme was used to calculate the vertex flux.

The scheme (54) describes the divergence-preserving method on general grids. The same construction is possible for the three-dimensional equations (44) yielding a three-dimensional scheme. We proceed by specifying (54) for triangular and rectangular grids. Note that the averaging using Nedelec elements does not give any information about preservation properties on the primary grid of cell mean values. We will uncover the preservation properties by identifying the resulting schemes with the schemes of the previous sections.

**6.3.2. Example: Triangles.** The scheme (54) is valid for any kind of grid for which averaged face elements are known. In this section we will consider triangles. If $P_i$ denotes the piecewise linear hat function that gives unity at vertex $p_i$ and zero at all other vertices, then the face element $\mathbf{W}_{K_{i,j,k}}^{\mathbf{e}_{i,j}}$ has the representation

$$\mathbf{W}_{K_{i,j,k}}^{\mathbf{e}_{i,j}} = |\mathbf{e}_{i,j}| \left( P_i \, (\operatorname{grad} P_j)^\perp - P_j \, (\operatorname{grad} P_i)^\perp \right) \Big|_{K_{i,j,k}}. \tag{56}$$

By writing the gradients explicitly, we obtain

$$\mathbf{W}_{K_{i,j,k}}^{\mathbf{e}_{i,j}}(x,y) = \frac{|\mathbf{e}_{i,j}|}{2\,|K_{i,j,k}|} \left( P_i(x,y)\, \mathbf{e}_{k,i} - P_j(x,y)\, \mathbf{e}_{j,k} \right), \tag{57}$$

which directly leads to the averages

$$\overline{\mathbf{W}^{\mathbf{e}_{i,j}}_{K_{i,j,k}}} = \frac{|\mathbf{e}_{i,j}|}{6\,|K_{i,j,k}|}\,(\mathbf{e}_{k,i} - \mathbf{e}_{j,k})\,. \tag{58}$$

Using this in (54) results in the scheme

$$\begin{aligned}\partial_t \mathbf{B}_{K_{i,j,k}} &= -\frac{(f_i\,\mathbf{e}_{j,k} + f_j\,\mathbf{e}_{k,i} + f_k\,\mathbf{e}_{i,j})}{2\,|K_{i,j,k}|} \\ &= \frac{\left(\frac{f_j+f_k}{2}\,\mathbf{e}_{j,k} + \frac{f_k+f_i}{2}\,\mathbf{e}_{k,i} + \frac{f_i+f_j}{2}\,\mathbf{e}_{i,j}\right)}{|K_{i,j,k}|},\end{aligned} \tag{59}$$

which is identical to the scheme given in (40). In (59) the relation $\mathbf{e}_{i,j}+\mathbf{e}_{j,k}+\mathbf{e}_{k,i}=0$ has been used to rearrange the terms. The equivalence to (40) becomes more evident by looking at the residual in (42) and the observation that $\frac{f_i+f_j}{2} = \langle f_{i,j}\rangle$ with $\langle f_{i,j}\rangle$ given in (43).

Since both schemes (59) and (40) are equivalent, we conclude that the scheme (59) shares the preservation properties of the flux distribution scheme (40). The scheme obtained by Nedelec averaging for triangles will exactly preserve the local values of the operators $\mathrm{div}^{(\star)}$ and $\mathrm{div}^{(+)}$ given in (32) and (34).

**6.3.3. Example: Rectangles.** For rectangles, the averaged face elements are given by

$$\overline{\mathbf{W}^{i+\frac{1}{2}}_{i,j}} = \begin{pmatrix} \frac{1}{2} \\ 0 \end{pmatrix},\ \overline{\mathbf{W}^{i-\frac{1}{2}}_{i,j}} = \begin{pmatrix} -\frac{1}{2} \\ 0 \end{pmatrix},\ \overline{\mathbf{W}^{j+\frac{1}{2}}_{i,j}} = \begin{pmatrix} 0 \\ \frac{1}{2} \end{pmatrix},\ \overline{\mathbf{W}^{j-\frac{1}{2}}_{i,j}} = \begin{pmatrix} 0 \\ -\frac{1}{2} \end{pmatrix} \tag{60}$$

for the four edges of the cell. The resulting averaging formulas have also been used in [4], [8], and [13] to obtain cell centered values of the magnetic flux density from the staggered variables.

From (54) follows the evolution scheme for the cell averages, which reads

$$\begin{aligned}\partial_t \mathbf{B}_{i,j} = \frac{1}{2\Delta x \Delta y}\Bigg( & f_{i+\frac{1}{2},j+\frac{1}{2}} \begin{pmatrix} \Delta x \\ -\Delta y \end{pmatrix} + f_{i-\frac{1}{2},j+\frac{1}{2}} \begin{pmatrix} \Delta x \\ \Delta y \end{pmatrix} \\ & + f_{i-\frac{1}{2},j-\frac{1}{2}} \begin{pmatrix} -\Delta x \\ \Delta y \end{pmatrix} + f_{i+\frac{1}{2},j-\frac{1}{2}} \begin{pmatrix} -\Delta x \\ -\Delta y \end{pmatrix}\Bigg),\end{aligned} \tag{61}$$

where $f_{i+\frac{1}{2},j+\frac{1}{2}}$ is given by (55), i.e., averaging of the intercell fluxes of the four adjacent edges. This method is the same as that of (24), which can be seen after making the averages $f_{i+\frac{1}{2},j+\frac{1}{2}}$ explicit.

The scheme in (24) exactly preserves the extended divergence operator (12); hence, as in the triangular case, this preservation holds also for the scheme based on Nedelec averaging. This leads to the conclusion: Assume that mean normal field components on edges in a rectangular grid are given and closed integrals over these normal components on the edges vanish; i.e., the premise in (51) is fulfilled. Then the evaluation of the extended divergence operator $\mathrm{div}^{(\star)}$ given in (12) on cell averages of the field found by Nedelec averaging (53) gives exactly zero. The analogous statement holds also for a triangular grid. This fact is an additional property of face element reconstructions, which is hard to obtain by the averaging formula (53) alone. Hence, if the Nedelec averaging approach is solely used to derive similar schemes for, say, quadrilateral grids, one would lack the knowledge of the precise divergence operator that is preserved.

**7. Conclusion.** New flux modifications have been presented that turn an arbitrary MHD finite volume method into a locally divergence-preserving finite volume scheme. That scheme belongs to the broad class of cell centered conservative (in the sense of volume integrals) schemes but additionally preserves the value of a certain discrete divergence operator in each volume cell and keeps the calculation free of divergence errors, as demonstrated in the numerical experiments. We deduced the necessary modifications for rectangular and triangular grids in two dimensions using the flux distribution framework presented in [33]. Special upwind weighting derived from characteristic information assure compact stencils, which results in sharper shock resolution. A special case of the schemes may be related to a staggered grid scheme, as presented in [4] and [34]. Additionally, an alternative construction uncovered the close relation between finite element method reconstruction with Nedelec elements and the newly derived divergence-preserving schemes. The construction via so-called Nedelec averaging provides also the possibility of extending the methods most easily to quadrilateral grids and three dimensions.

The advantages of the new schemes are clear: They mimic the analytical properties of the induction equation by preserving the divergence in each time step. The divergence preservation is built directly into the fluxes. Hence, there is no need for a staggered grid and/or a cleaning procedure after each time step. Furthermore, the original MHD equations are solved without artificial production terms, and the upwind weighting produces sharper shock wave resolutions.

The next step could be to incorporate the method into an adaptive framework on rectangular grids. In [2] and [35] restriction and prolongation formulas are given for the magnetic flux density stored in a staggered grid. In our case there is need for similar formulas which, however, use cell averages and preserve the extended divergence operator given in (12).

**Acknowledgment.** The author would like to thank Dr. M. Fey (ETH Zürich, Switzerland) for valuable discussions and suggestions.

REFERENCES

[1] M. Alcubierre, G. Allen, B. Brugmann, E. Seidel, and W.-M. Suen, *Towards an understanding of the stability properties of the* 3+1 *evolution equations in general relativity*, Phys. Rev. D (3), 62 (2000), article 124011.

[2] D. S. Balsara, *Divergence-free adaptive mesh refinement for magnetohydrodynamics*, J. Comput. Phys., 174 (2001), pp. 614–648.

[3] D. S. Balsara, *Second order accurate schemes for magnetohydrodynamics with divergence-free reconstruction*, Astrophys. J. Suppl., 151 (2004), pp. 151–184.

[4] D. S. Balsara and D. S. Spicer, *A staggered mesh algorithm using high order Godunov fluxes to ensure solenoidal magnetic fields in magnetohydrodynamic simulations*, J. Comput. Phys., 149 (1999), pp. 270–292.

[5] J. U. Brackbill and D. C. Barnes, *The effect of nonzero* $\nabla \cdot B$ *on the numerical solution of the magnetohydrodynamic equations*, J. Comput. Phys., 35 (1980), pp. 426–430.

[6] F. Brezzi and M. Fortin, *Mixed and Hybrid Finite Element Methods*, Springer-Verlag, New York, 1991.

[7] M. W. Choptuik, *Consistency of finite-difference solutions of Einstein's equation*, Phys. Rev. D, 44 (1991), pp. 3124–3135.

[8] W. Dai and P. R. Woodward, *On the divergence-free condition and conservation laws in numerical simulations for supersonic magnetohydrodynamic flows*, Astrophys. J., 494 (1998), pp. 317–335.

[9] A. Dedner, D. Kroener, C. Rohde, and M. Wesenberg, *MHD instabilities arising in solar physics: A numerical approach*, in Hyperbolic Problems: Theory, Numerics, Applications, H. Freistühler and G. Warnecke, eds., Birkhäuser, Basel, 2002, pp. 277–286.

[10] A. Dedner, F. Kemm, D. Kroener, C.-D. Munz, T. Schnitzer, and M. Wesenberg, *Hyperbolic divergence cleaning for the MHD equations*, J. Comput. Phys., 175 (2002), pp. 645–673.

[11] H. De Sterck, *Multi-Dimensional Upwind Constrained Transport on Unstructured Grids for Shallow Water Magnetohydrodynamics*, AIAA paper 2001-2623, 2001.

[12] D. L. De Zeeuw, T. I. Gombosi, C. P. T. Groth, K. G. Powell, and Q. F. Stout, *An adaptive MHD method for global space weather simulations*, IEEE Trans. Plasma Sci., 28 (2000), pp. 1956–1965.

[13] C. R. Evans and J. F. Hawley, *Simulation of magnetohydrodynamic flows: A constrained transport method*, Astrophys. J., 332 (1988), pp. 659–677.

[14] M. Fey, *Multidimensional upwinding. Part* I. *The method of transport for solving the Euler equations*, J. Comput. Phys., 143 (1998), pp. 159–180.

[15] M. Fey, *Multidimensional upwinding. Part* II. *Decomposition of the Euler equations into advection equations*, J. Comput. Phys., 143 (1998), pp. 181–199.

[16] E. Godlewski, and P.-A. Raviart, *Numerical Approximation of Hyperbolic Systems of Conservation Laws*, Springer, New York, 1996.

[17] J. J. Gonzalez, R. Girard, and A. Gleizes, *Decay and post-arc phases of a SF*6 *arc plasma: A thermal and chemical non-equilibrium model*, J. Phys. D, 33 (2000), pp. 2759–2768.

[18] G. Guj and F. Stella, *A vorticity-velocity method for the numerical solution of* 3*D incompressible flow,* J. Comput. Phys., 106 (1993), pp. 286–298.

[19] J. M. Hyman and M. Shashkov, *Natural discretizations for the divergence, gradient, and curl on logically rectangular grids*, Comput. Math. Appl., 33 (1997), pp. 81–104.

[20] A. Jeffrey and T. Taniuti, *Non-linear Wave Propagation*, Academic Press, New York, 1964.

[21] G.-S. Jiang and C.-W. Shu, *Efficient implementation of weighted ENO schemes*, J. Comput. Phys., 126 (1996), pp. 202–228.

[22] J. Jin, *The Finite Element Method in Electrodynamics*, Wiley-Interscience, New York, 1993.

[23] S. Lenzner, M. Auweter-Kurtz, J. Heiermann, and P. C. Sleziona, *Energy partitions in inductively heated plasma sources for reentry simulations*, J. Thermophys. Heat Transfer, 14 (2000), pp. 388–395.

[24] R. Limacher, *Simulation der MHD-Gleichungen mit der Transportmethode*, diploma thesis, ETH Zurich, 2000.

[25] S.-J. Lin and R. B. Rood, *An explicit flux-form semi-Lagrangian shallow-water on the sphere*, Quart. J. Roy. Meteor. Soc., 123 (1997), pp. 2477–2498.

[26] K. W. Morton and P. L. Roe, *Vorticity-preserving Lax–Wendroff-type schemes for the system wave equation*, SIAM J. Sci. Comput., 23 (2001), pp. 170–192.

[27] C.-D. Munz, P. Omnes, R. Schneider, E. Sonnendrucker, and U. Voss, *Divergence correction techniques for Maxwell solvers based on a hyperbolic model*, J. Comput. Phys., 161 (2000), pp. 484–511.

[28] J. C. Nedelec, *Mixed finite elements in* $\mathbb{R}^3$, Numer. Math., 35 (1980), pp. 315–341.

[29] S. Noelle, *The MoT-ICE: A new high-resolution wave-propagation algorithm for multidimensional systems of conservation laws based on Fey's method of transport*, J. Comput. Phys., 164 (2000), pp. 283–334.

[30] K. G. Powell, *An Approximate Riemann Solver for Magnetohydrodynamics (That Works in More Than One Dimension)*, ICASE report 94-24, 1994.

[31] K. G. Powell, P. L. Roe, T. J. Linde, T. I. Gombosi, and D. L. DeZeeuw, *A solution-adaptive upwind scheme for ideal magnetohydrodynamics*, J. Comput. Phys., 154 (1999), pp. 284–309.

[32] T. Sonar, *Methods on unstructured grids, WENO and ENO recovery techniques*, in Hyperbolic Partial Differential Equations, A. Meister and J. Struckmeier, eds., Vieweg, Braunschweig, 2002, pp. 115–232.

[33] M. Torrilhon and M. Fey, *Constraint-preserving upwind methods for multidimensional advection equations*, SIAM J. Numer. Anal., 42 (2004), pp. 1694–1728.

[34] G. Toth, *The* $\nabla \cdot B$ *constraint in shock-capturing magnetohydrodynamics codes*, J. Comput. Phys., 161 (2000), pp. 605–652.

[35] G. Toth and P. L. Roe, *Divergence- and curl-preserving prolongation and restriction formulas*, J. Comput. Phys., 180 (2002), pp. 736–750.

[36] M. Wesenberg, *Efficient MHD Riemann solvers for simulations on unstructured triangular grids*, J. Numer. Math., 10 (2002), pp. 37–71.